

Modeling of optical coupling to multimode polymer waveguides: Axial and lateral misalignment tolerance

Guoyu Yu and David R. Selviah

Department of Electronic and Electrical Engineering, University College London,
Torrington Place, London WC1E 7JE, United Kingdom
g.yu@ee.ucl.ac.uk, d.selviah@ee.ucl.ac.uk

Abstract: BPM modeling establishes a set of design curves for coupling loss of a VCSEL optical source for several widths of square multimode polymer waveguides giving the interdependence of lateral and axial offset misalignments.

Introduction

10 Gb/s optical multimode polymer waveguide links [1,2] for optical backplanes in racks of printed circuit boards can have the active devices such as VCSELs and photodiodes mounted on the daughterboards to allow them to be more easily replaced in the event of device failure. The backplane then consists of polymer waveguides fabricated on a printed circuit board yielding a robust arrangement. However, this approach requires the lasers and photodiodes to be aligned to the backplane waveguides precisely in optical connectors. The daughterboards plugged into the backplane may carry vibrating components such as hard disc drives so it is essential that the optical connection between the boards is tolerant to relative misalignments. VCSEL optical sources give good tolerance with multimode waveguides [1,2]. In this paper we investigate the influence of waveguide width on the efficiency of power coupling by modeling, Figure 1. Our model takes account of the spatial distribution of the VCSELs optical field and calculates the coupling to the waveguide modes. In long fibers or single mode waveguides the coupling can be considered independently at the waveguide ends. However, in short waveguides a misaligned laser affects the spatial distribution of optical power at the photodiode waveguide end. Conversely, a misaligned photodiode can affect the coupling characteristics of the laser. Therefore, we investigate (Fig. 1) the effect of translational axial misalignments, Δz_t parallel to the waveguide and lateral misalignments, Δx_t normal to the waveguide for laser sources when combined with lateral misalignments, Δx_r of the photodiodes at the receiver.

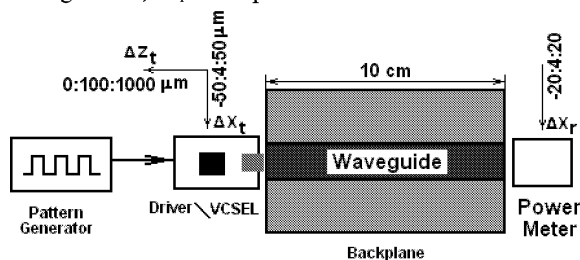


Fig. 1 Optical waveguide link model block diagram

Optical waveguide link modeling

The temporal characteristics of the 850 nm wavelength 10 Gb/s VCSEL, linearly polarized along the +Y axis were modeled using laser rate equations [3]. 10 Gb/s VCSELs can support 4 transverse modes [1] which due to their spatial frequencies give a beam divergence of 20°. The divergence of the optical source affects its waveguide coupling characteristics. In order to obtain results of general validity

which are not dependent on the actual relative amplitudes and phases of the 4 transverse modes we used a single lowest order VCSEL mode with a Laguerre-Gaussian spatial distribution, Fig. 2(a) but scaled it down in size to a $1/e^2$ width of 3.1 μm to give the correct divergence of 20°.

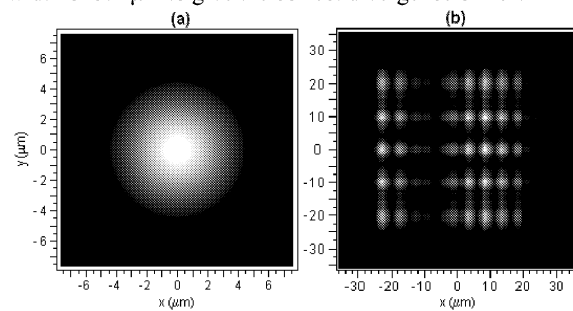


Fig. 2 Spatial optical intensity distribution (a) of the VCSEL and (b) of the waveguide at the photodiode, $\Delta x_t = +18 \mu\text{m}$, $\Delta z_t = 0 \mu\text{m}$, $\Delta x_r = +8 \mu\text{m}$

The thermal characteristics and drive current dependencies were captured using experimentally measured free space LI curves at a range of temperatures for a 10 Gb/s VCSEL provided by the manufacturers. However, our calculations effectively used a small signal laser model since we neglected transverse mode hops in the spatial optical field distribution of the VCSEL. The VCSEL was biased using a 5 mA DC current. The modulation was provided by an additional 5 mA monopolar NRZ 10^{10} -1 long PRBS of pulses having rise/fall times of 40/45 ps respectively, specified at 32 points. Typical laser driver RIN of -130 dBm, jitter of 8 ps and VCSEL bond wire parasitics, 0.3 nH, 1.5pF, were assumed with typical values for receiver thermal, shot and dark current noise. The multimode polymer waveguide had a square core with a refractive index of 1.54 and cladding index of 1.51 giving an NA of 0.3. The loss was taken to be 0.03 dB/cm at 850 nm. This loss is typical of measured guides and consists of material loss, volume scattering loss and wall roughness scattering loss. The spatial field distribution was calculated using a forward propagating, wide angle, finite difference beam propagation method (FD-BPM) with (1,1) Padé coefficients and reflections were neglected. The waveguide was 10 cm length, typical of lengths expected on the backplane [2]. The calculation domain was from -60 μm to +60 μm . The calculation grid was reduced in spacing until it no longer affected the results which gave a 0.2 μm spaced transverse grid and a 6 μm spaced axial grid. This gave 16 points across the input light distribution. A 75 μm diameter 10 GHz bandwidth photodetector placed in contact with the end of the waveguide averaged the output optical field.

Results and Discussion

One of the output optical field distributions calculated is shown in Fig. 2 (b) for the misalignments $\Delta x_t = +18 \mu\text{m}$, $\Delta z_t = 0 \mu\text{m}$, $\Delta x_r = +8 \mu\text{m}$. The BPM model calculates the output including the effect of interference between the multiple modes of the waveguide but neglecting the important effect of finite coherence length. A periodic grid of smeared copies of the input can be observed reminiscent of a Fresnel diffraction pattern through a square aperture rather than being a random speckle pattern. The horizontal pitch is smaller than the vertical pitch and depends on the amount of laser offset. It is known from work on planar slab light guides that multiple copies of the input light source are seen in a periodic arrangement and this appears to be similar but in two dimensions due to the 2D guide. Simulations were performed starting with the VCSEL in contact with the entrance face of the waveguide and moving it axially out to $\Delta z_t = 1000 \mu\text{m}$, in steps of $100 \mu\text{m}$. For each value of Δz_t the VCSEL was moved laterally from $\Delta x_t = -50 \mu\text{m}$ to $+50 \mu\text{m}$ in steps of $4 \mu\text{m}$. In addition, at each location of the VCSEL the photodiode was moved laterally from $\Delta x_r = -20 \mu\text{m}$ to $+20 \mu\text{m}$ in steps of $4 \mu\text{m}$. There is a trade-off between coupling loss and misalignment tolerance so to obtain the largest tolerance we assume that the maximum coupling loss that can be tolerated is 2 dB overall, due to the two connections, which may not be equally divided between the connectors. In Fig. 3 we plotted contours of a total link loss of 2 dB for square waveguides of several widths. Fig. 3(a) has no photodiode offset while Figs 3(b) has a photodiode offset of $+8 \mu\text{m}$. The contours show that larger width waveguides have more lateral and axial misalignment tolerance. The lateral tolerance increases slightly with axial offset first before decreasing. The axial tolerance $2\Delta x_t$ is much larger than the lateral tolerance Δz_t by a factor of about 10. Our results do not show a minimum loss of 2 dB for $50 \mu\text{m}$ square guides at an axial position of $400 \mu\text{m}$ observed experimentally in [4] but do agree that for $75 \mu\text{m}$ square guides the lowest loss is achieved at $\Delta z_t = 0 \mu\text{m}$. The contours for guide widths of 10, 20, 30, 40 and $50 \mu\text{m}$ do not depend on photodiode offset as seen by comparing Fig 3(a) and (b). However, for guide widths above $50 \mu\text{m}$ the contours appear to become unstable and do not change shape uniformly with changes in either waveguide width or with changes in photodiode offset. These effects are related to the size of the photodetector relative to the guide width. If the photodetector has an aperture much larger than the waveguide then any photodiode offsets will still allow the photodiode to capture all of the energy. If the photodiode has a slightly larger diameter than the waveguide small photodiode offsets do not have much effect but larger offsets leave a gap at the side of the photodiode through which light passes missing the photodiode. In fig 3(b) the $60 \mu\text{m}$ waveguide width shows a small change due to the $0.5 \mu\text{m}$ gap while the $70 \mu\text{m}$ waveguide width shows the larger effect of the $5 \mu\text{m}$ gap. If the photodetector has a smaller aperture than the waveguide it only receives part of the light distribution shown in figure 2(b) with a gap around the photodiode resulting in increased loss and modal noise due to VCSEL mode partition noise or change of coupling to various waveguide modes due to misalignment of the connector or waveguide vibration which would change the optical spatial field at the output of the waveguide. To avoid

interdependence between the alignments of the components at each end of the waveguide the photodiode should cover the full area of the end of the waveguide at the maximum photodiode offset anticipated. Modal noise is reduced by ensuring that the mode selective loss is distributed equally between several connectors [5] but these results do not show the loss separately at each end of the waveguide.

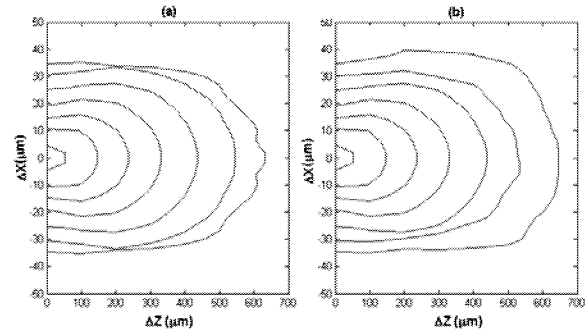


Fig. 3 Misalignment tolerance 2 dB link loss contours for square waveguides widths from inner to outer contours 10, 20, 30, 40, 50, 60, 70 μm . (a) $\Delta x_r=0$, (b) $\Delta x_r=+8 \mu\text{m}$

Using the guide's field distribution of Fig.2(b) together with modal dispersion of a circular fiber with the same length and diameter as the square waveguide we calculate the eye diagram, Fig. 4 for $\Delta x_t = +18 \mu\text{m}$, $\Delta z_t = 0 \mu\text{m}$, $\Delta x_r = +8 \mu\text{m}$ after the receiver's 10 GHz bandwidth raised cosine filter to minimize ISI. An eye opening of 40 mV is achieved.

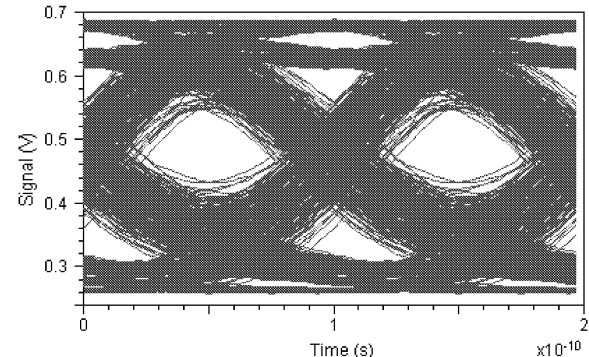


Fig. 4 Eye diagram $\Delta x_t = +18 \mu\text{m}$, $\Delta z_t = 0 \mu\text{m}$, $\Delta x_r = +8 \mu\text{m}$.

Acknowledgements

The authors thank EPSRC and DTI via the LINK Storlite Project and Xyratex Technology for financial support. Thanks also to Ioannis Papakonstantinou and F. Anibal Fernandez for useful discussions.

References

1. P. Pepeljugoski et al., *J. Lightwave Technol.*, vol. 21, pp. 1256-1275, 2003.
2. G. K. Chang et al., "Chip-to-chip optoelectronics SOP on organic boards or packages", to be published in *IEEE Trans. On Advanced Packaging*, July 2004.
3. V. N. Morozov et al., *IEEE J. Quantum. Electron.*, vol. 33, pp. 980-988, 1997.
4. T. Rupp, *EOS Optics in Computing*, Engelberg, 2004.
5. Daniel Kuchta et al., *Optical and Quantum Electron.*, vol. 27, pp. 203-223, 1995.